JOURNAL OF GEOPHYSICAL RESEARCH, VOL. 111, G04008, doi:10.1029/2006JG000181, 2006

Large-scale climatic patterns control large lightning fire occurrence in Canada and Alaska forest regions

Marc Macias Fauria[1,2] and Edward A. Johnson[3]

Received 10 February 2006; revised 20 April 2006; accepted 25 June 2006; published 15 November 2006.

[1] Large lightning wildfires in Canada and Alaska account for most of the area burnt and are main determiners of the age mosaic of the landscape. Such fires occur when positive midtroposphere height anomalies persist > 10 days during the fire season. Midtroposphere anomalies are part of teleconnections which are created by atmospheric and coupled sea/air dynamics. Large lightning fire occurrence and area burnt data were used to define eight centers of large wildfire variability in Canada and Alaska during 1959–1999. Preferred positions of persistent positive midtroposphere anomalies correlated with the Fire Regions during large fire events. Active fire weather showed strong relations with Pacific Decadal Oscillation (PDO) at interdecadal timescales and with El Niño Southern Oscillation (ENSO) and Arctic Oscillation (AO) mostly at interannual (2 to 6 years) timescales. PDO and ENSO (AO) related large fires were more frequent in the western (eastern) regions. The mountain ranges in western Canada play a major role in the large-scale patterns of large fire occurrence through retention of PDO-related Pacific Ocean moisture, causing the dynamics of large fires each side of the ranges to be mostly in antiphase. The PDO/ENSO regime shift of 1976/1977, together with the strong and persistent positive phase of AO during the late 1980s and 1990s contributed to the increase in area burned in the study area except in British Columbia and Alaska. PDO-ENSO-AO interactions with active fire weather provide an explanation for changes in large fire occurrence frequency during the last centuries in the area.

Citation: Macias Fauria, M., and E. A. Johnson (2006), Large-scale climatic patterns control large lightning fire occurrence in Canada and Alaska forest regions, *J. Geophys. Res.*, *111*, G04008, doi:10.1029/2006JG000181.

1. Introduction

[2] Forests of Canada and Alaska are a mosaic of different ages since they last burned [*Johnson*, 1992]. Lighting fires caused >85% of the area burned in these forests during 1959–1999 [*Stocks et al.*, 2002] (also Bureau of Land Management, Alaska Fire Service, 2003, http://agdc.usgs.gov/data/blm/fire/), and 14% of all fires accounted for 77% of the area burned [*Stocks et al.*, 2002]. Thus a few large fires shape the forest age mosaic.

[3] Changes in the fire frequency will alter the average age of the forest as a whole and will have major consequences in the carbon cycle of the biosphere-atmosphere [*Levine*, 1996]. Past changes in fire frequency (i.e., probability of an area burning per unit time) have been documented over large areas of the Canadian boreal forest and have been attributed to changes in climate, such as the end of the Little Ice Age [*Masters*, 1990; *Johnson and Larsen*, 1991; *Bergeron and Archambault*, 1993; *Larsen*, 1997; *Weir et al.*, 2000; *Bergeron et al.*, 2001; *Carcaillet et al.*, 2001].

[4] Annual area burned in Canada increased in the last decades of the 20th century [*Skinner et al.*, 1999, 2002; *Stocks et al.*, 2002]. General Circulation Models have been used to predict higher fire danger levels in a global change scenario based on an increase in temperatures over North America [*Stocks et al.*, 1998]. Recent studies have linked human-induced climatic change through emissions of greenhouse gases and an increase in area burned by forest fires in Canada over the past 4 decades [*Gillett et al.*, 2004]. However, it is very important to identify and describe the mechanisms leading to large-scale patterns of fire occurrence before predicting future trends in area burned under global-change scenarios.

[5] Large lightning fires are associated with persistent (>10 days) positive midtroposphere (500 hPa) anomalies (upper air blocking highs) that block zonal atmospheric circulation [*Schroeder et al.*, 1964; *Finklin*, 1973; *Janz and Nimchuk*, 1985; *Street*, 1985; *Flannigan and Harrington*, 1986; *Johnson and Wowchuk*, 1993; *Skinner et al.*, 1999, 2002]. During these events, lack of precipitation and prevailing meridional flow of warm air rapidly dry fuel over large areas. Fuel dryness, as measured by the Canadian Fire Behavior System [e.g., *Johnson and Wowchuk*, 1993], associates strongly with persistent positive midtroposphere

[1]Department of Ecology, University of Barcelona, Barcelona, Spain.
[2]Also at Department of Biological Sciences, University of Calgary, Calgary, Alberta, Canada.
[3]Department of Biological Sciences, University of Calgary, Calgary, Alberta, Canada.

0148-0227/06/2006JG000181$09.00

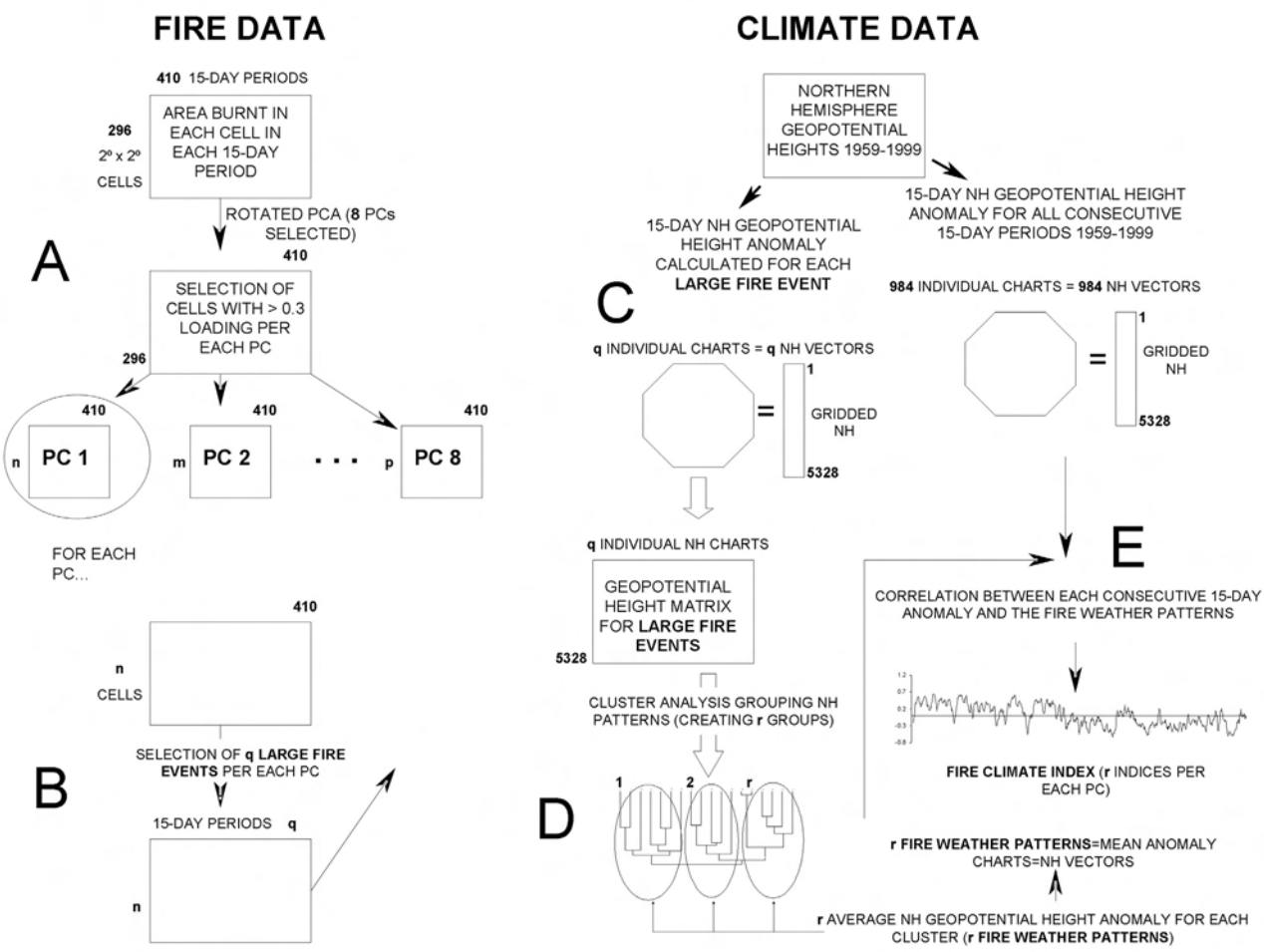

Figure 1. Flowchart indicating the general structure and organization of the methods followed in this study. (a) Fire data arrangement and multivariate analysis. (b) Selection of large fire events. (c) Midtroposphere geopotential height data arrangement and calculation of midtroposphere height anomalies during large fire events. (d) Grouping of large fire events height anomalies by cluster analysis and calculation of fire weather upper air patterns. (e) Calculation of fire climate Indices. PC, principal component; NH, Northern Hemisphere; squares, data matrices; octagons, NH charts.

anomalies, providing a causal explanation for potential of large fires.

[6] Such persistent positive midtroposphere anomalies are in turn associated with teleconnection patterns. Relations between temperature and precipitation in North America and teleconnections, such as the interannual El Niño–Southern Oscillation (ENSO), the Pacific Decadal Oscillation (PDO), the Pacific North American teleconnection (PNA), the Atlantic multidecadal oscillation (AMO), the Arctic Oscillation (AO) as well as global sea-surface temperatures (SST) have been reported [*Yarnal*, 1984; *Ropelewski and Halpert*, 1986, 1987; *Kiladis and Díaz*, 1989; *Trenberth and Branstator*, 1992; *Zhang et al.*, 1997; *Shabbar et al.*, 1997; *Minobe*, 1997; *Bonsal and Lawford*, 1999; *Rajagopalan et al.*, 2000; *Zhang et al.*, 2000; *Thompson and Wallace*, 2001; *Enfield et al.*, 2001; *Shabbar and Skinner*, 2004; *Coulibaly and Burn*, 2005; *Knox and Lawford*, 1990; *Hoerling and Kumar*, 2003].

[7] Long-term modifications of the atmospheric flow due to large-scale climatic changes could modify these circulation patterns, modifying the spatial and temporal occurrence of large fires. Our purpose is to identify the relations between large-scale climatic fluctuations and large fire occurrence in Canadian and Alaskan forests, focusing on the climatic conditions that lead to fuel drying over large areas and hence to higher potential for large area burned.

[8] Previous studies have linked teleconnection patterns and large fire occurrence in Canada [*Skinner et al.*, 1999, 2002] and Alaska [*Hess et al.*, 2001; *Duffy et al.*, 2005]. However, no analysis has been made of large area burnt patterns for both Canada and Alaska. Further, the temporal divisions have been made on monthly to annual fire data and not at a scale that corresponds to the midtropospheric patterns. Spatially, landscape has been divided into political or eco-regions [e.g., *Flannigan et al.*, 2005]. Focusing on time and space scales implies taking into account the causal mechanisms of large forest fire occurrence (midtroposphere anomalies and ultimately teleconnection patterns) and their scales. By doing so, results are made easier to interpret and to link to physical processes, and strong relations between climate and area burnt are found. Thus a study giving a

comprehensive continental picture of large fire occurrence on the boreal forest of North America focusing on the time and spatial scale of large forest fires is necessary.

[9] In this study we show that (1) large lightning fires have recurrent spatiotemporal patterns or fire regions, (2) these fire regions are correlated with positions of positive midtroposphere anomalies, (3) fire-related positive midtroposphere anomalies are part of hemispheric teleconnections that determine their position and thus affect fire occurrence over the study area at both high (interannual) and low (interdecadal) frequencies and (4) teleconnection interactions with large fire occurrence suggest explanations for known past changes in large-fire occurrence and fire frequency during the last 3 centuries.

2. Data

[10] Lightning-caused large (>200 ha) fires for Canada and Alaska from 1959 to 1999 were obtained from the Canadian Large Fire Database [*Stocks et al.*, 2002] and the Alaska Historical Fire Database (Bureau of Land Management, Alaska Fire Service; http://agdc.usgs.gov/data/blm/fire/). Data include information on fire location, start date and final size of fires.

[11] Data of the mean daily geopotential height of the midtroposphere (500 hPa) for the Northern Hemisphere were obtained from the NCEP Reanalysis database, provided by the NOAA-CIRES Climate Diagnostics Centre, Boulder, Colorado, USA http://www.cdc.noaa.gov/ [*Kalnay et al.*, 1996]). These data have a spatial coverage of 2.5 degrees latitude $\times$ 2.5 degrees longitude, resulting in a 144 $\times$ 37 cell grid for the Northern Hemisphere.

[12] Data of three teleconnection indices expected to affect active fire weather over the study area were used. (1) The Arctic Oscillation (AO) [*Trenberth and Paolino*, 1981; *Wallace and Gutzler*, 1981] is defined as the dominant mode of sea level pressure (SLP) north of 20°N, is characterized in its positive (negative) phase by negative (positive) pressure anomalies over the Arctic and a circumpolar belt of positive (negative) anomalies at mid latitudes. AO index data were obtained from the National Ocean and Atmospheric Administration (NOAA; http://www.cpc.noaa.gov/). (2) El Niño 3 time series consists of the sea surface temperature (SST) between 5°N–5°S and 150°W–90°W and represents ENSO variability. ENSO records were obtained from the Joint Institute for the Study of the Atmosphere and Ocean (JISAO) data archive at the University of Washington (http://tao.atmos.washington.edu/). (3) The Pacific Decadal Oscillation (PDO) is the leading mode of monthly SST anomalies in the North Pacific Ocean, poleward of 20°N http://tao.atmos.washington.edu [*Zhang et al.*, 1997; *Hare*, 1996; *Mantua et al.*, 1997]). PDO events persisted for 20 to 30 years during the 20th century. Warm (cool) PDO phases were characterized by a strengthened (weakened) Aleutian low enhancing (reducing) the advection of warmer air onto the west coast of North America, which caused positive (negative) temperature anomalies over northern North America, with a maximum (minimum) anomaly located over central Canada [*Minobe*, 1997; *Mantua and Hare*, 2002]. Warm PDO phases tend to produce persistent high-pressure anomalies over northern North America, especially over western Canada and Alaska [*Zhang et al.*, 1997]. PDO is related to the SST, precipitation and convection variability in the Indian Ocean and tropical Pacific, and its spatial climatic patterns are similar to the ENSO pattern [*Mantua et al.*, 1997; *Zhang et al.*, 1997). The physical mechanisms responsible for the PDO are not fully understood [*Mantua and Hare*, 2002], but tropical proxy data connected to the PDO [*Evans et al.*, 2000, 2001; *Linsley et al.*, 2000] suggest an interaction with climate in the tropics and Southern Hemisphere.

3. Methods

[13] A flowchart in Figure 1 is presented that summarizes the methods used in this study.

3.1. Identifying Fire Regions

[14] Orthogonally rotated principal component analysis (VARIMAX criterion [*Kaiser*, 1958]) based on the correlation matrix of the fire data was used to define the primary spatiotemporal patterns of large lightning fire variability (fire regions). Such an approach has been applied in climatological studies to identify climate regions [*Richman and Lamb*, 1985, 1987; *Serreze et al.*, 1998]. This method was adopted in our study because it is able to establish the major spatial patterns (or modes) of variability of large fire occurrence and has been previously shown to work on rather episodic data sets such as convective rainfall [*Richman and Lamb*, 1985], which show similar structure to our data set.

[15] The study area was divided into a 2° latitude $\times$ 2° longitude grid. Cells were excluded from analysis if no lightning-caused fire >200 ha occurred during 1959–1999. The resulting grid consisted of 296 cells (auxiliary material[1] Figure S1). Grid cell size was chosen to include several large fires during the 41-year period, as well as to allow enough spatial resolution for fire regions to be defined. Fire season was set to May–August (i.e., the period when large fires in the study area mostly occur) and was divided into successive 15-day periods, resulting in ten 15-day periods per season, and a series of 410 15-day periods from 1959–1999. The 15-day resolution largely coincides with the duration of blocking highs that result in years of large fires [*Johnson and Wowchuk*, 1993] and also matches the Duff Moisture Code drying rate model [*Van Wagner*, 1987], which represents moisture in the layer of loosely compacted decomposing matter on the forest floor, with a nominal depth of approximately 7 cm. The area burned in each cell was log-transformed to reduce its skewness.

[16] Thus, variables in the PCA were the area burned in each 2° $\times$ 2° cell (296), and observations or cases were the 15-day periods (410) (Figure 1a). Prior to rotation, a number of principal components were selected by observing the decline in successive eigenvalues (scree plot) and also by considering whether the components were interpretable [*Rummel*, 1970]. In our case, interpretable refers to a regional pattern of the variable loadings for each principal component (i.e., high loadings mainly concentrate in a defined geographical region). Lines of longitude converge toward the pole so the 2° $\times$ 2° grid cells that we used do not represent a fixed

[1] Auxiliary materials are available in the HTML. doi:10.1029/2006JG000181.

area. To assess the effect of the resulting unequal sampling, we compared separate rotated principal component analysis for the south and north and east and west halves of the study area [cf. *Richman and Lamb*, 1985].

[17] Principal component loadings (i.e. correlations between the time series of area burned in each cell –variable- and the time series of the principal component scores) were interpreted as a probability surface defining the spatial pattern of large fire occurrence, with each loading associated with a $2^\circ \times 2^\circ$ cell. Component loadings >0.3 were selected to define the regional boundaries of the fire regions, selecting thus a number (n) of cells or variables (Figure 1a) per component.

3.2. Fire Regions and Northern Hemisphere Midtroposphere Circulation Patterns

[18] Large fire events were identified as the 15-day periods with the largest area burnt; a number q of large fire events was selected per fire region (Figure 1b) until 70% of the total area burned during 1959–1999 in each fire region was accounted for. Next, we identified the date when the largest fires began during each large fire event (M_d) as an indicator of enough forest fuel dryness over a fire region to facilitate a large fire, i.e., the day after at least 10 days of fair weather produced by an upper air blocking high.

[19] Northern Hemisphere 500 hPa geopotential heights for the 15 days prior to each M_d were obtained and mean 15-day height charts were produced (q charts per fire region; Figure 1c); next, Northern Hemisphere geopotential height anomalies were computed as the difference from the 41-year 500 hPa height climatological mean for each 15-day period prior to M_d. Mean 500 hPa height increases during summer over northern North America, peaking during the latter half of July and then decreasing rapidly. This means different climatological 500 hPa height means during the fire season. In addition, the mean geopotential height varies regionally. Because of both sources of variation, raw height anomalies cannot be compared for the entire study area and period. Thus each 500 hPa height anomaly corresponding to a large fire event was normalized with respect to its regional climatology by $N = (X - \mu)/\sigma$, where X is a grid point 15-day mean height, μ is the grid point 41-year climatological height mean and σ the standard deviation. The magnitude of the normalized anomaly is thus given in standard deviations [cf. *Grumm and Hart*, 2001; *Xue et al.*, 2003].

[20] The q geopotential height anomaly charts in each fire region were then grouped into similar 500 hPa height anomaly patterns (Figure 1d) by using a correlation-based unweighted pair-group average (UPGMA) cluster analysis [*Sneath and Snokal*, 1973]. Clusters were defined using a Type 1 error rate of 0.001, which corresponded to $r \sim 0.04$ ($n > 5000$). This produced a number r of groups of similar geopotential height anomaly charts per each fire region. Finally, an average 500 hPa Northern Hemisphere chart was produced for each resulting cluster in each fire region (named fire weather upper air pattern). This produced a number r of fire weather upper air patterns per fire region. Each individual standardized 15-day anomaly height was weighted according to its total area burned during averaging. As an example, if an area of 100,000 ha was burned during the 15-day period A, and an area of 80,000 ha was burned during the 15-day period B on a given fire region, then the weighting scheme would give the period A anomaly height a relative weight of 1 and the period B a relative weight of 0.8 in the averaging process.

[21] To construct a set of time series or fire climate indices for each fire region describing the potential for large fires (i.e., active fire weather), a running mean was computed which correlated each fire weather upper air pattern with the upper air pattern of any 15-day geopotential height average during all months of the year from 1959 to 1999 (Figure 1e). That is, we calculated as many fire climate indices as fire weather upper air patterns (i.e., r fire climate indices per fire region). According to this procedure, high correlation coefficients correspond to 15-day periods with mean upper air height anomaly patterns similar to the fire weather upper air pattern. Therefore high (low) fire climate indices imply high (low) potential for large fires over a given fire region. The resulting r time series had 984 consecutive values each (every 15-day period for 1959–1999; Figure 1e).

[22] Fire climate indices were used to search for trends in the occurrence of midtroposphere patterns favorable to large fires, as well as to test their relation to the teleconnection indices thought to affect the incidence of large fires over the study area: El Niño–Southern Oscillation (ENSO), the Pacific Decadal Oscillation (PDO) and the Arctic Oscillation (AO). Many time series in geophysics exhibit nonstationarity in their statistics: While the series may contain dominant periodic signals, these signals can vary in both amplitude and frequency over time. Wavelet analyses attempt to solve these problems by decomposing time series into time-frequency space simultaneously, representing their frequency content while still keeping the time description parameter. A Morlet wavelet approach [*Torrence and Compo*, 1998; *Grinsted et al.*, 2004] was used to assess such relations. Our analysis involved continuous wavelet transform (CWT), Cross wavelet transform (XWT) and wavelet coherence transform (WCT). CWT is a common and powerful tool for analyzing intermittent oscillations in a time series. Such analyses have edge artifacts that are accounted for by defining a cone of influence (COI), outside which edge effects can be ignored. XWT calculates the common power between two series and their relative phase in the time-frequency space, whereas WCT measures the coherence of the cross wavelet transform in the time-frequency space; it is usefully thought of as a localized correlation coefficient in the time-frequency space. Phase angle statistics were used to gain confidence in causal relations among the time series [*Jevrejeva et al.*, 2003; *Grinsted et al.*, 2004]. Significance of wavelet power and coherence was assessed following the procedures of *Grinsted et al.* [2004].

[23] Wavelet analyses were limited by the relatively short length of the series (41 years), so that long-term variability could not be assessed by this procedure. As an alternative method to assess the interannual and interdecadal variability associated with the relations between Fire Climate Indices and teleconnection indices, 7-year centered unweighted moving averages were computed, generating 35-year long low-pass-filtered series and the corresponding 35-year long high-pass-filtered series

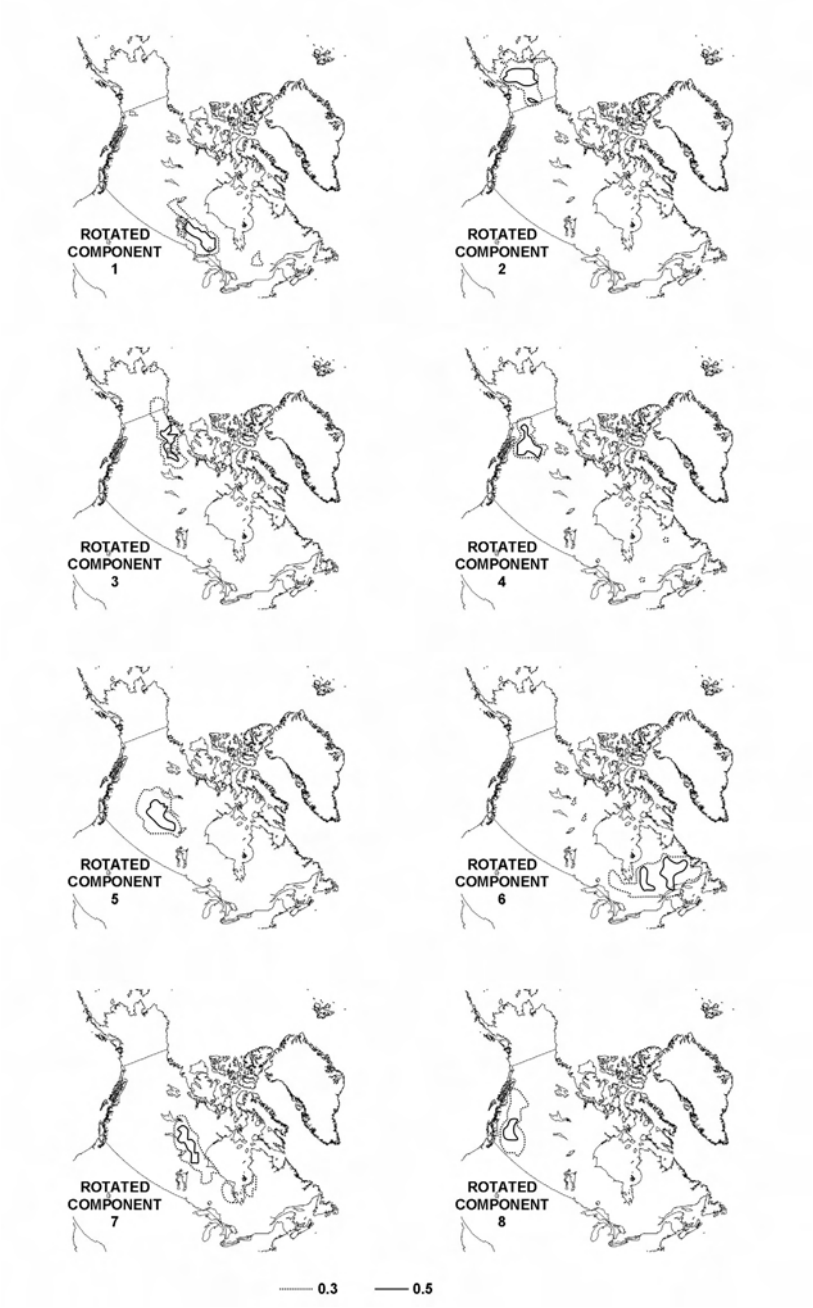

Figure 2. The 0.3 and 0.5 component loading isopleths of the VARIMAX orthogonally rotated principal components 1–8 of the correlation matrix of the Alaska and Canada large fire data, derived from log-transformed 15-day totals for all $2^\circ \times 2^\circ$ grid cells for the May–August periods of 1959–1999. The resulting regions (whose boundaries are the 0.3 loading isopleths for each PC) are called fire regions: rotated component (RC) 1, South Central; RC 2, Alaska; RC 3, Northwest Territories; RC 4, Yukon; RC 5, West Central; RC 6, East; RC 7, Central; RC 8, British Columbia.

obtained by subtracting the 7-year low-pass-filtered series from the original series.

4. Results

4.1. Fire Regions in Canadian and Alaskan Forests

[24] Eight principal components, explaining 24.7% of the entire domain (common) variance, were selected for rotation This is a rather high percentage, given the high time resolution of the fire data (15-day periods), the large number of variables used (and hence PCs obtained – 296) and the episodic nature of fire data, resulting in many observations with a value of zero. For example, *Walsh and Mostek* [1980] found that the first 10 out of 61 possible unrotated principal components explained 50% of the variance in U.S monthly station precipitation, and *Diaz* [1981] found that the first 5 of 48 principal components accounted for 58% of the variance in a similar analysis. In our case, 2.7% of all

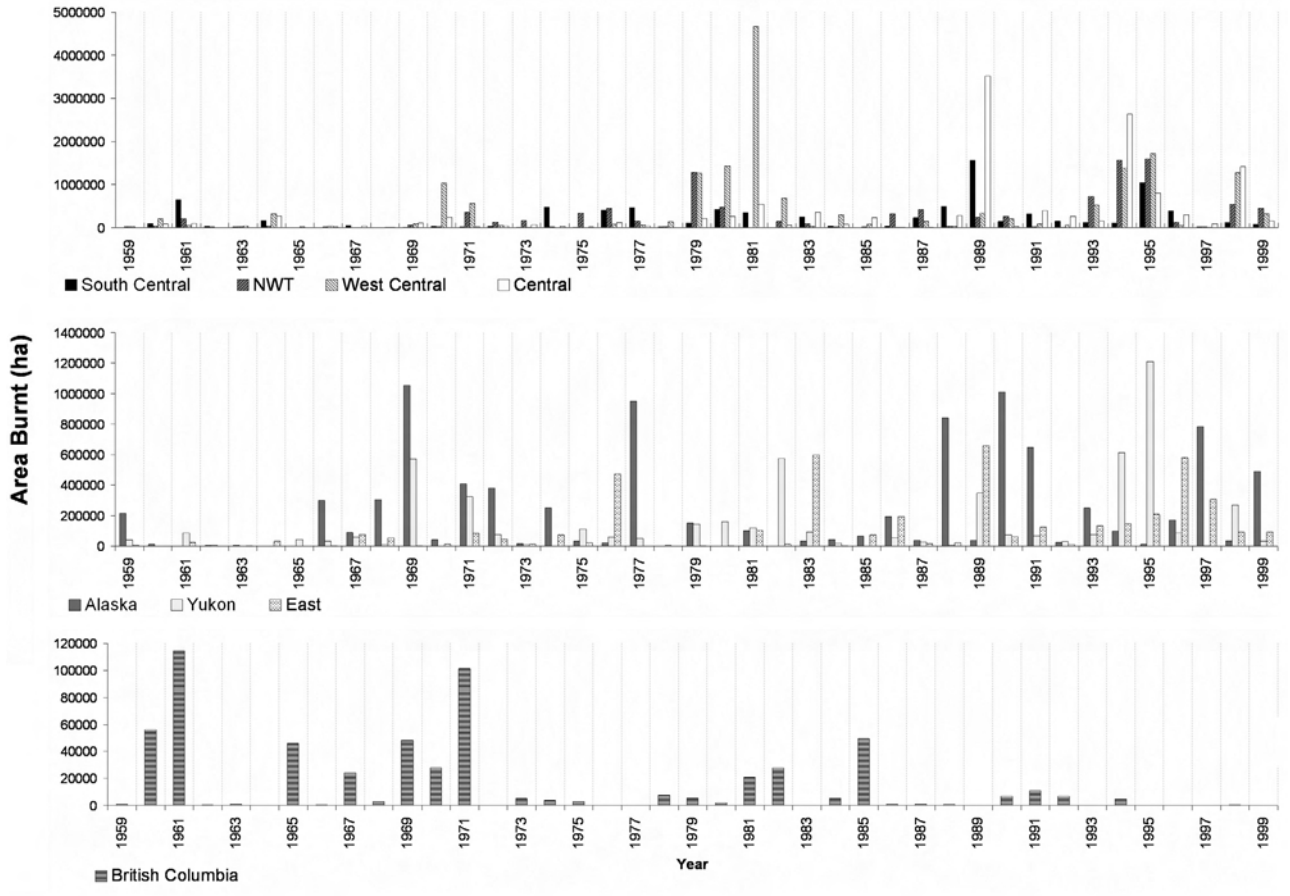

Figure 3. Area burnt per year by lightning-caused fires in each fire region.

principal components accounted for 24.7% of the common variance, resulting in ratio of common variance versus % of selected PC of 9.1; the ratios for the two examples given above are 3.1 and 5.6, respectively.

[25] Thus forested areas in Canada and Alaska were divided into eight fire regions according to the occurrence of large, lightning fires, based on the spatial distribution of the component loadings larger than 0.3 for each rotated principal component (Figure 2). Fire regions cover > 94% of the total area burned during the record and are largely nonoverlapping (88.5% of their total area did not overlap).

[26] Analyses of the east and west halves and north and south halves of the study area yielded very similar loading patterns, supporting the coherence of the identified fire regions and indicating negligible effects of the decrease in cell size with latitude. No principal component represented eastern and southern Ontario and southern Québec, or south and south-eastern Alaska and coastal northern British Columbia, due to the low area burned in these areas during the record.

[27] During 1959–1999, all fire regions showed area burnt totals in the millions of hectares (from 4.4 million in East to 17.4 million in Central) except British Columbia (~0.6 million). The annual area burnt increased in all fire regions, except British Columbia, which showed the opposite pattern, and Alaska, which did not show any major trend (Figure 3). In many cases, individual years or clusters of years with very large area burnt occurred. The late 1980s and early 1990s contained several large fire years in all regions east of the Rocky Mountains.

4.2. Fire Regions and Northern Hemisphere Midtroposphere Circulation Patterns

[28] Thirteen to 26 large fire events were found in each fire region (i.e., 4–5% of all 15-day periods accounted for ~70% of the total area burned). Three to four fire weather upper air patterns were defined for each fire region (Table 1). The first two fire weather upper air patterns for each fire region (auxiliary material Figures S2a–S2d) accounted for an average of 87% of the total area burned by large fire events (Table 1), whereas the remaining ones accounted for infrequent situations (2 to 5 large fire events in 41 years) with generally no significant area burned (not shown).

[29] Fire weather upper air patterns were defined at a hemispheric scale by the dominant patterns of midtropospheric geopotential height in the tropics, the Arctic and the midlatitudes (Table 1). Four general types of fire weather upper air patterns were identified. We will name these types referring to the teleconnections they were strongly associated with, as shown later. The PDO/ENSO + (−) type is characterized by both widespread positive (negative) height anomalies in tropical regions and low (high) heights over the Northern Pacific. AO + Type involves generalized low geopotential heights over the Arctic Ocean and a belt of positive height anomalies at midlatitudes with the exception of frequent lows west of Canada's Pacific coast, i.e., deep

Table 1. Fire Weather Upper Air Patterns for Each Fire Region[a]

Fire Region Number and Name	Fire Region Versus Blocking High Position	NH Type	Main Circulation Features		Main Height Anomaly Patterns			Large Fire Events			Special Features
			WCR	CPT	Tropic	Arctic	Midlatitude Belt	Number	Percent Area Burnt	Time	
1. South Central	centered	3	eastward	-	-	low	high	15	65.7	since 1976	
	centered/ downstream	2	strong eastward	weak	low	high	-	6	22.8	before 1976	low in Gulf of Alaska, highs in central N Pacific
	downstream	1	strong eastward	-	high	high	low	5	11.5	after 1976 (May)	
2. Alaska	southern part	4	-	-	-	high	low (50°N–65°N)	6	39.9	no pattern	belt of highs at 30°N–50°N
	centered	1	strong northwestward	deep	high	-	-	5	35.5	since 1976	lows in N Pacific "wavy" circulation
	centered	3	weak northwestward	weak	-	low	high	4	13	since 1988	
	centered	2	weak northwestward	-	low	-	-	3	11.7	before 1976	strong ridging over Fennoscandia, deep trough U.S.A southeast
3. NWT	centered	1	northeastward	deep	high	-	low	14	74.8	since 1976	troughs in Bering Sea and western Siberia, highs in China
	southern part	4	weak	-	-	high	low	3	25.2	no pattern	belt of highs 30°N
4. Yukon	centered	1	northward	-	high	low	-	7	62.6	since 1976	troughs in Bering Sea, Siberia and Azores
	centered	3	-	weak	-	low	high	6	24.1	since 1988	highs in eastern Canada
	downstream	2	weak		low	high	-	4	13.4	before 1976	
5. West Central	downstream	1	westward	-	high	low	-	11	42.4	since 1976	trough in central Pacific and W Atlantic
	downstream	1	westward	-	high			5	36.9	1981	4.5×10^6 ha burnt in one fire season highs in W Bering Sea and Siberia
	n.p.	3	weak	-	-	low	high	3	20.7	no pattern	highs in eastern Canada
6. East	centered	3	-	eastward	-	low	high	7	54.7	since 1976	trough in U.S.A. southeast and Gulf of Alaska, highs in Bering Sea and western Europe
	downstream	1	westward	-	high	low		7	39.6	since 1976	trough in U.S.A. southeast, E Atlantic and W Pacific
	southern part	1	-	-	high	-	-	2	5.7	after 1990	
7. Central	centered	3	eastward	-	high	-	-	12	78.0	since 1976	trough in U.S.A. southeast, western Pacific
	southern part	1	strong westward	-	high	high	-	4	16.3	since 1976	trough in central North America Ridge in Labrador Peninsula
	n.p.	2	-	-	low	-	-	3	5.7	no pattern	highs in U.S.A. southeast, N Atlantic
8. British Columbia	centered	2	strong	weak	low	high	-	8	68.6	before 1976	
	northern part	1	-	-	high	-	-	3	21.9	1985 and 1969	
	centered	3	weak	weak	-	low	high (40°N)	2	9.5	1981 and 1970	

[a]NH type: Northern Hemisphere fire weather upper air pattern type where 1 is PDO/ENSO +, 2 is PDO/ENSO −, 3 is AO + and 4 is AO −. In Main Circulation Features, WCR (CPT) refers to the Western Canadian Ridge (Canadian Polar Trough) position and/or strength. In Main Height Anomaly Patterns, general height anomaly patterns are described for the tropical, arctic and midlatitude regions. In Large Fire Events, Number refers to the number of Large fire events that defined the fire weather upper air pattern, % Area Burnt refers to the proportion of the total fire weather upper air pattern–related area burnt in the fire region and Time defines any temporal pattern of large fire events occurrence during 1959–1999; n.p. denotes not present.

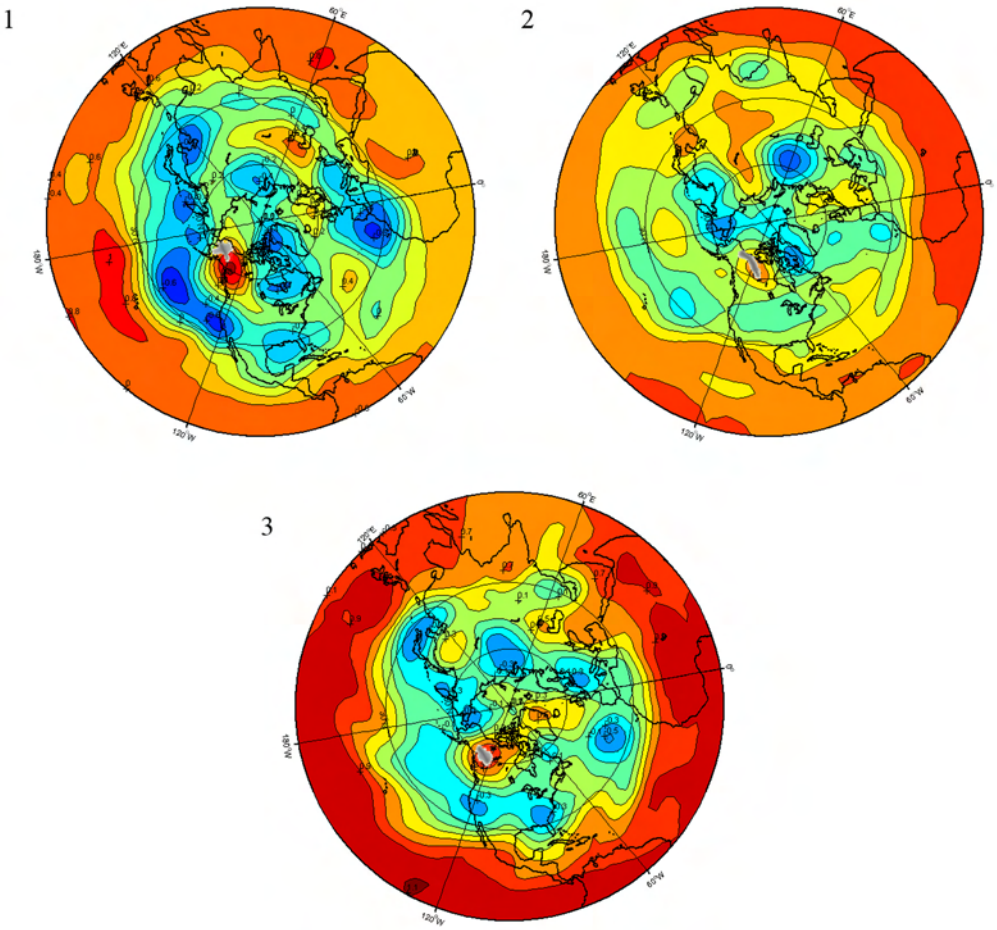

Figure 4. Northern Hemisphere 500 hPa height anomaly charts for fire weather upper air patterns in (a) Alaska, (b) Northwest Territories and (c) Yukon. Fire regions are highlighted. Charts define upper air conditions prone to active large fire weather in each fire region for the PDO/ENSO + type of fire weather upper air pattern. Light shades (cold colors): low geopotential height anomalies; dark shades (warm colors): high geopotential height anomalies. Units are in standard deviations. Note that the position of the fire-related upper air highs differs in each fire region, whereas the general Northern Hemisphere upper air height patterns are similar.

West Coast Trough. Finally, AO − type presents positive upper air height anomalies over the Arctic Ocean, surrounded by a belt of lows at mid-high latitudes (centered ∼50°N–60°N) and a belt of highs at lower latitudes (centered at ∼30°N).

[30] Fire weather upper air patterns were defined regionally (Table 1) by the position of positive midtroposphere geopotential heights in relation to the fire region as well as by the midtroposphere height patterns over the Northern Pacific Ocean, and the strength and position of the Western Canadian Continental Ridge (WCR) [*Skinner et al.*, 2002] and the Canadian Polar Trough (CPT) [*Shabbar et al.*, 1997]. Eastward and northward expansions of WCR were responsible for most fire-related midtroposphere highs (Table 1 and auxiliary material Figures S2a–S2d). Positive 500 hPa geopotential height anomalies in all fire weather upper air patterns were consistently centered above or upstream (relative to the main upper air stream) the fire regions [see also *Johnson and Wowchuk*, 1993; *Skinner et al.*, 1999, 2002]. Figure 4 shows three fire weather upper air patterns corresponding to the PDO/ENSO + type for Alaska, Northwest Territories and Yukon fire regions.

[31] PDO/ENSO + patterns accounted for 48% of the total area burned by large fire events and were related to fire regions east of the Canadian Rocky Mountains, especially in the western half of the study area, where they accounted for >80% of the area burnt. Such events mainly occurred after 1976 (Table 1). PDO/ENSO - patterns accounted for 7% of the total area burnt and were related primarily to large fires in British Columbia and, to a lesser degree, in Yukon and South Central Regions. Such events mainly occurred prior to 1976 (Table 1). AO + patterns accounted for 35% of the area burned by large fire events and were especially related to large fires in the eastern half of Canada, where they accounted for > 68%. Such events mainly occurred after 1976 (Table 1). Finally, AO − patterns accounted for 9% of the total area burnt and were related to fires occurring mainly in Alaska and the Northwest Territories, where they

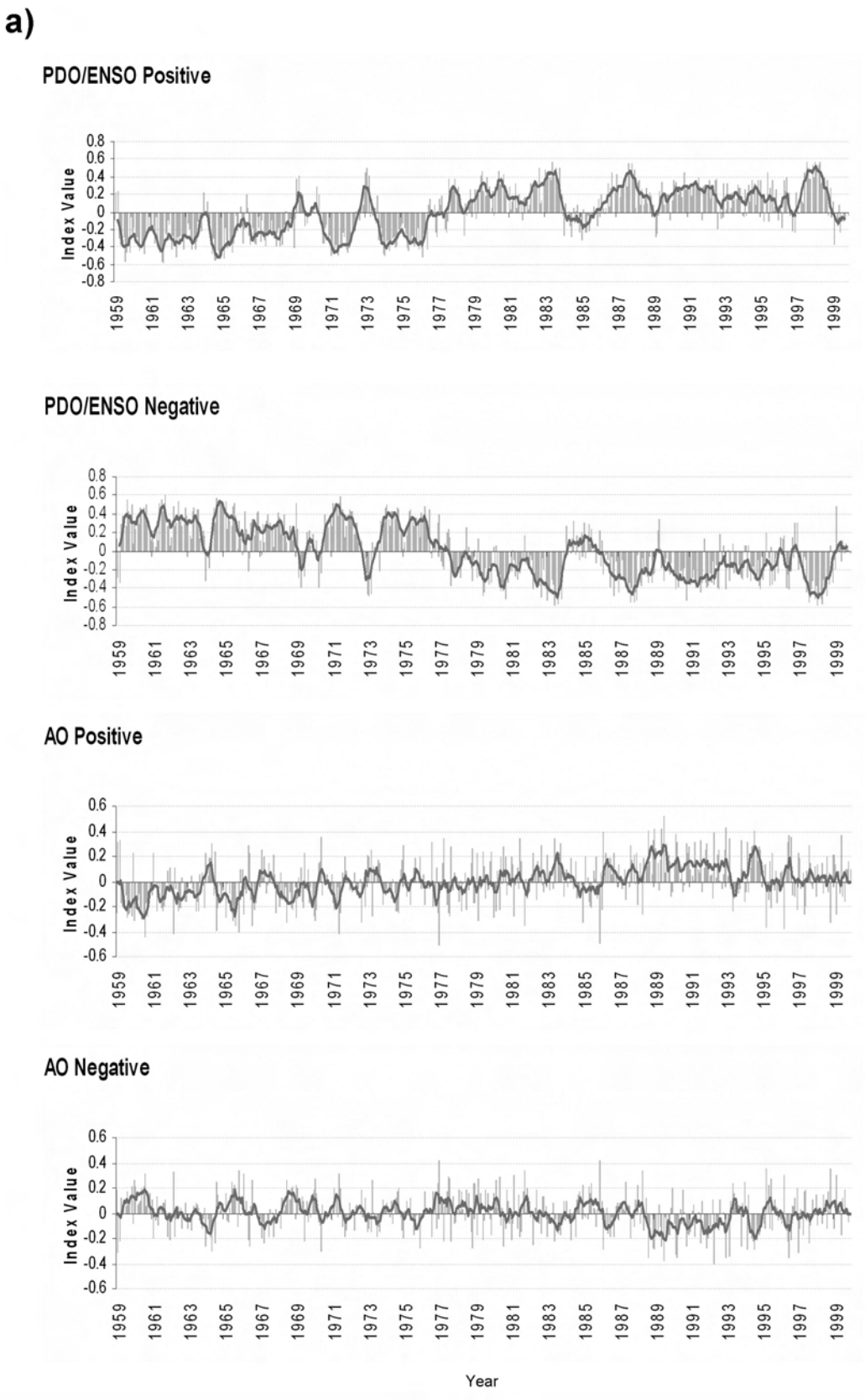

Figure 5a. Monthly fire climate indices types, each one resulting from a type of fire weather upper air pattern: PDO/ENSO +, PDO/ENSO −, AO + and AO −. Fire climate indices are time series describing the potential for large fires related to a fire weather upper air pattern over a given fire region during 1959–1999. Continuous thick line shows a 6-month smoothed average.

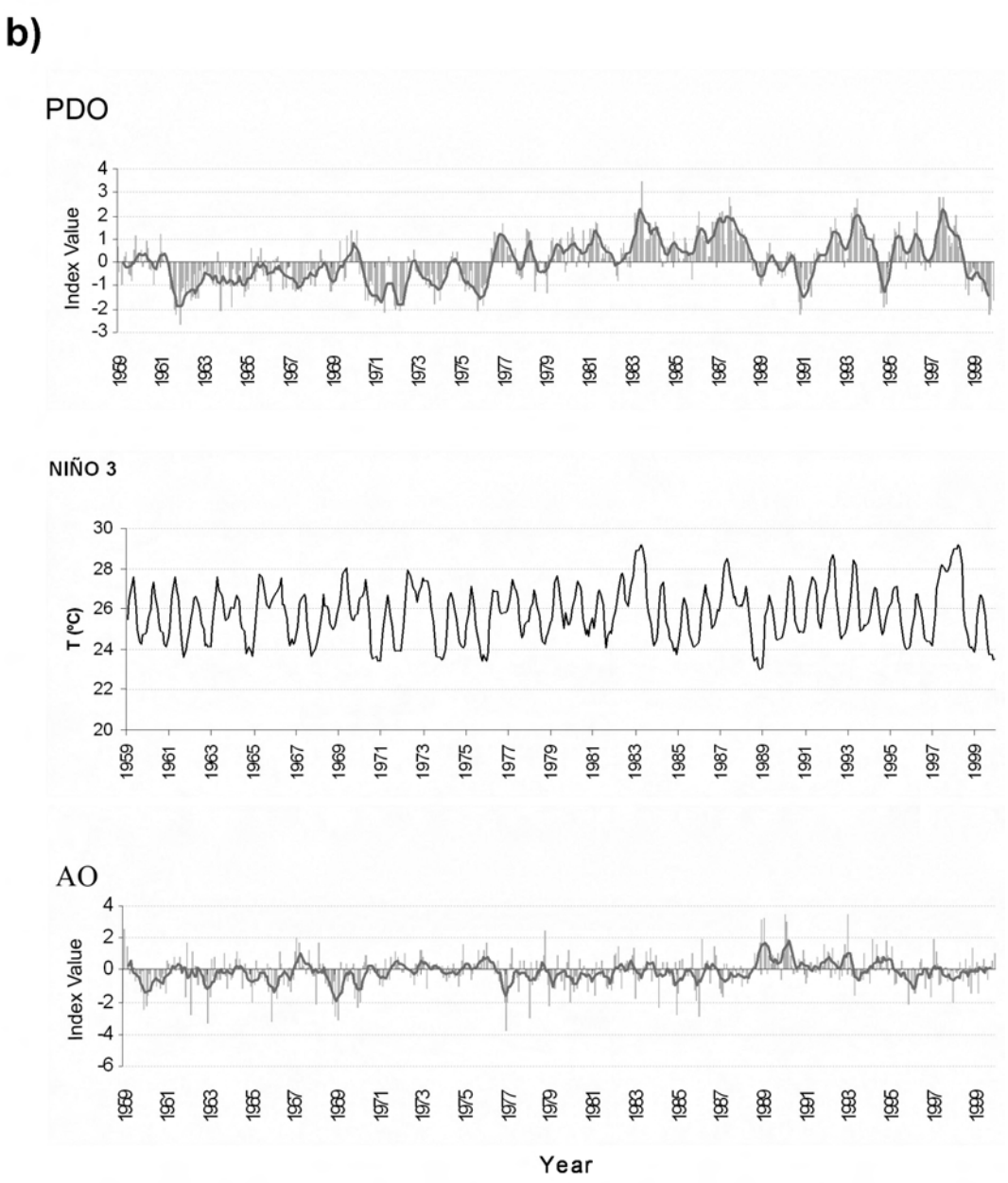

Figure 5b. Monthly Pacific Decadal Oscillation (PDO), Niño 3 and Arctic Oscillation (AO) time series for 1959–1999. Continuous thick line shows a 6-month smoothed average.

accounted for ~ 40% and 25% of the area burnt, respectively, and did not show any specific temporal pattern of occurrence during the period.

4.3. Fire Climate Indices

[32] Twenty-four Fire Climate indices were computed, one for each fire weather upper air pattern (8 fire regions x *r* in Figure 1d). They were easily grouped into 4 types of fire climate indices, each corresponding to one of the Northern Hemisphere height pattern types described in the previous section. Averaged PDO/ENSO +, PDO/ENSO −, AO + and AO − fire climate indices are shown in Figure 5a. PDO/ENSO + (−) fire climate indices were characterized by low interannual variability and negative (positive) and persistent values from 1959 to 1976, with brief exceptions in 1969 and 1973, followed by a sharp regime shift in 1976–1977 and very positive (negative) and persistent index values from then to 1999. The 1976–1977 shift matches a major change in large fire occurrence occurred around 1976. AO + (−) fire climate indices were characterized by high interannual variability and dominance of negative (positive) values during the first decades (1960s and 1970s) and positive (negative) index values during the last decades (1980s and 1990s) of the period 1959–1999.

[33] No large fires occurred during periods of low fire climate indices (i.e., low potential for large fire occurrence), and large fire events were consistently associated with periods of high index values. However, not all high fire

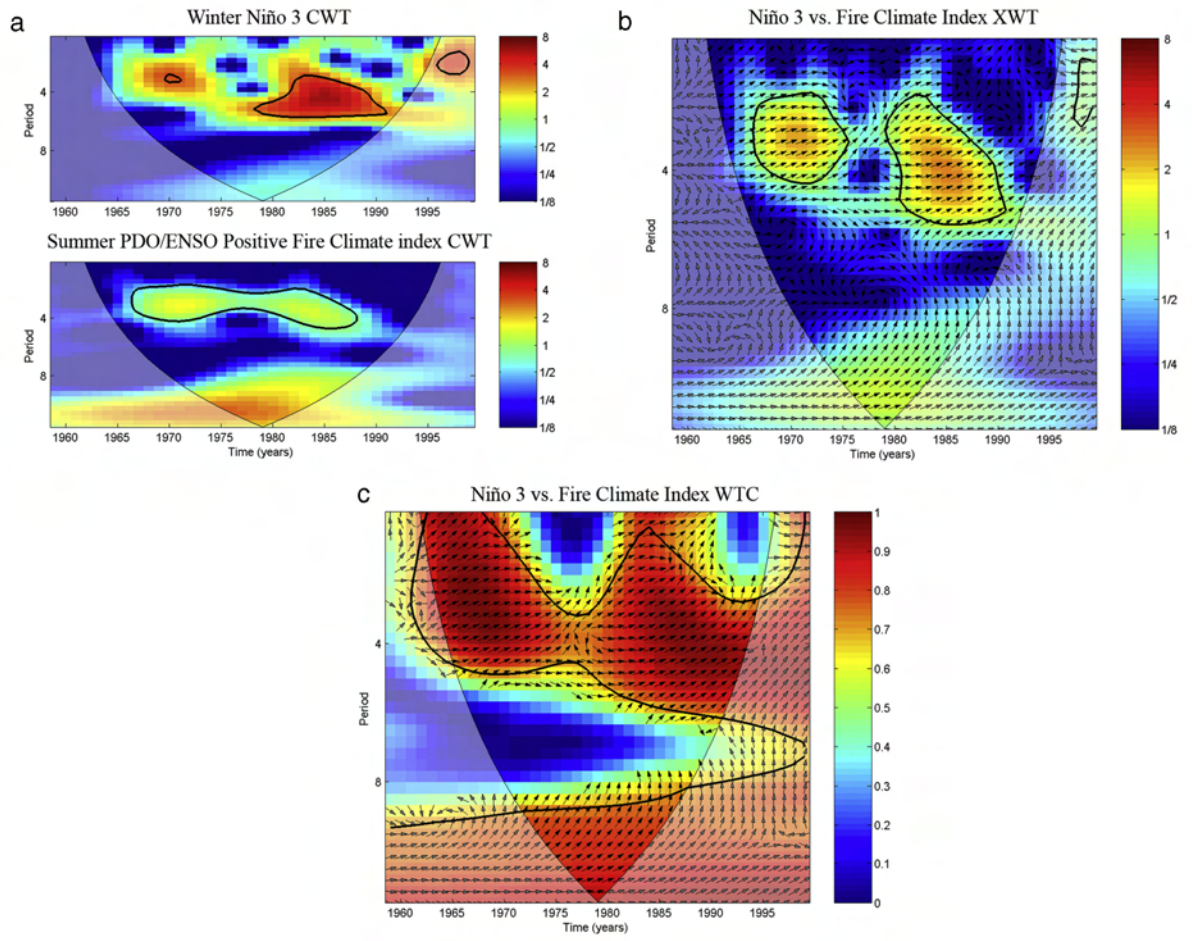

Figure 6. (a) Continuous Wavelet Power spectrum of the normalized (top) winter Niño 3 time series and (bottom) summer PDO/ENSO + type fire climate index. (b) Cross wavelet transform (XWT) of the two time series in Figure 6a. (c) Squared wavelet coherence (WCT) between the two time series in Figure 6a. The thick black contour designates the 5% significance level against red noise and the cone of influence, which defines where edge effects are important, is shown as a lighter shade. The relative phase relationship in XWT and WCT is shown as arrows (with in-phase pointing right, antiphase pointing left, and Niño 3 leading fire climate index by 90° pointing straight up). Graphs for the types negatively related to ENSO are shown in Auxiliary material S4a.

climate index values corresponded to large area burnt (e.g., auxiliary material Figure S3).

4.4. Fire Climate Indices and Teleconnection Patterns

[34] PDO/ENSO + (−) fire climate indices were found to be strongly and positively (negatively) correlated with PDO and ENSO through all months of the year during 1959–1999. Fire climate indices typically lagged behind PDO by 2 to 5 months. For PDO, the average index from March to August (spring-summer) explained most of the variability of fire climate indices during the fire season; whereas for El Niño 3 series the average index from January to March (winter) was most important. AO + (−) fire climate indices correlated strongly and positively (negatively) with AO through all months of the year during 1959–1999. No lag was detected in these relations.

[35] Wavelet analyses were performed on the normalized series of summer fire climate indices, spring-summer PDO and winter Niño 3, as well as on the summer AO series. ENSO and PDO showed consistent in-phase (antiphase) relations with PDO/ENSO + (−) fire climate indices, whereas AO showed consistent in-phase (antiphase) relations with AO + (−) fire climate indices.

[36] Winter Niño 3 showed significant common power with summer PDO/ENSO + and − fire climate indices at ~2- to 6-year frequency bands (typical ENSO frequency band [*Minobe*, 2000]) during 1966–1975 and 1978–1990 (Figure 6 and auxiliary material Figure S4a). Wavelet coherence showed significant linkages in the 2–6 year and the > 8-year bands during the whole period. A coherence and common wavelet power minimum occurred at high frequencies during 1976–1977.

Table 2. Correlations Between the 7-Year High- and Low-Pass-Filtered Summer Fire Climate Indices Shown in Figure 5a and the Teleconnections With Which They are Associated, Shown in Figure 5b[a]

Filtered Series	Fire Climate Index	PDOsp-sm	Niño 3 wt
High-pass series	PDO/ENSO positive	0.27	0.76
	PDO/ENSO negative	−0.25	−0.74
Low-pass series	PDO/ENSO positive	0.72	0.19
	PDO/ENSO negative	−0.73	−0.19
Series Filtered	Fire Climate Index	AO sm	
High-pass series	AO positive	0.84	
	AO negative	−0.82	
Low-pass series	AO positive	0.24	
	AO negative	−0.35	

[a]Abbreviations: sp-sm, spring-summer; wt, winter. Period is 1962–1996.

[37] Cross wavelet analyses performed with spring-summer PDO and summer PDO/ENSO + and − fire climate indices (auxiliary material Figures S4b and S4c) showed ENSO-like strong common power at interannual frequency bands, but interdecadal variability typically associated with the PDO was not detectable due to the short length of the time series (41 years). High-pass-filtered fire climate indices captured most of the variability associated with El Niño-ENSO cycle, whereas low-pass-filtered series captured the interdecadal variability associated with the PDO (Table 2).

[38] Summer AO showed significant common power at high frequencies (<4 years) with AO + and − fire climate indices for the periods 1965–1975 and from 1985 onward. Coherence was significant during the record at high frequencies (Figure 7 and auxiliary material Figure S4d), and also at a ~8-year band, especially with AO − fire climate

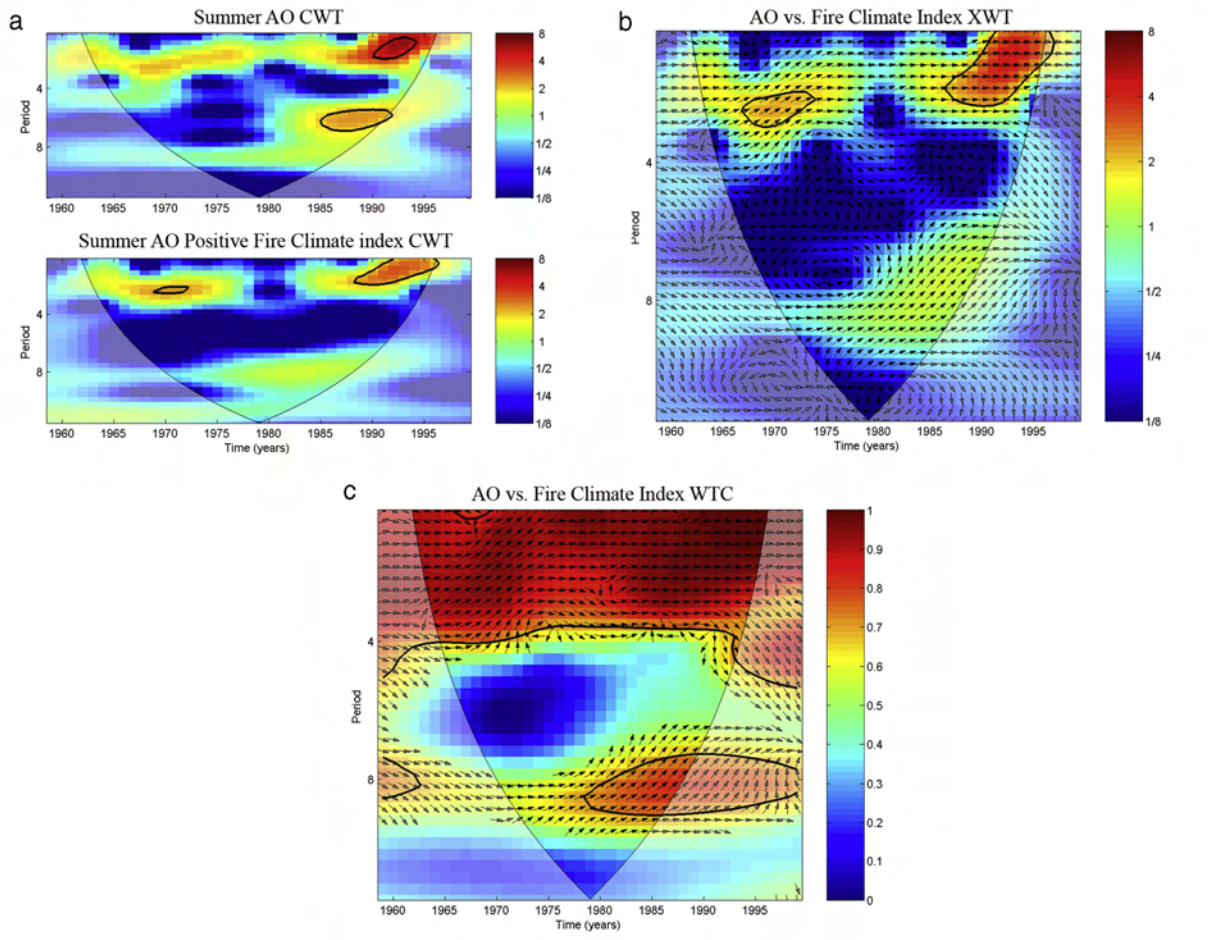

Figure 7. As in Figure 6 but for normalized summer AO and summer AO + type fire climate index. Graphs for the types negatively related to AO are shown in auxiliary material S4d.

Table 3. Phase Angle Statistics for Fire Climate Indices and Teleconnections[a]

	Circular Angle, °	Circular SD, °	Angle Strength
PDO/ENSO positive versus PDOsp-sm	−41.30	26.10	0.90
PDO/ENSO positive versus Niño3 wt	−29.70	20.65	0.94
PDO/ENSO negative versus PDOsp-sm	140.66	27.13	0.90
PDO/ENSO negative versus Niño3 wt	150.88	21.41	0.93
AO Positive versus AO sm	−11.21	24.54	0.91
AO Negative versus AO sm	173.18	21.15	0.93

[a]Circular angle is mean phase angle (in °) over the regions with significant wavelet coherence and outside the cone of influence (as in Figures 6/7) between Fire Climate Index Types and summer AO, spring-summer PDO and winter ENSO for 1959–1999. Circular SD is circular standard deviation of the Circular Angle (in °). Angle strength is measure of the consistency of the phase angles through the time frequency- space. Angle strength varies between 0 and 1 and can be thought of as the inverse of the variance of all phase angles.

indices. Fire season–summer-AO (positive and negative) fire climate indices and summer AO showed stronger relations at interannual than at interdecadal variability, as seen in the low-pass- and high-pass-filtered series correlations (Table 2).

[39] Fire climate indices lagged AO, ENSO and PDO (i.e., teleconnection patterns lead fire index patterns; Table 3). However, AO and AO + (−) fire climate indices were practically in total phase (antiphase), and so it was not possible to determine which index was leading despite the small standard deviation of the phase angles in the time-frequency domain, as they occurred almost simultaneously.

5. Discussion

[40] The occurrence of large, lightning-caused fires varied in Canada and Alaska among eight fire regions during 1959–1999 (Figure 2). Their sizes suggest that large-scale factors determined their positions. Fire regions reflect persistent positive midtroposphere anomalies at specific locations over North America, and were located consistently below or at the downstream part of such anomalies during large fire events (Table 1, Figure 4, and auxiliary material Figures S2a–S2d).

[41] That areas known to have had large fires in the past (Southern Ontario, Southern Québec and northwestern coastal forests [e.g., *Bergeron et al.*, 2001]) did not show large areas burned during the record, together with the occurrence of 6 fire events encompassing several (>2) contiguous fire regions during the 41-year record, suggests that fire occurrence and area burnt may be interacting at different time and space scales.

[42] We have focused our analysis on the conditions leading to fuel drying and thus to a higher probability of large fire occurrence; that is, in the weather patterns during the 2 weeks prior to the start of a large lightning fire. However, dry conditions are not the only weather factor required for large fire occurrence: Thunderstorm activity and lightning strikes after a dry period are needed for the onset of such fires [*Nash and Johnson*, 1996]. We have not directly addressed this issue in our study, but it is logical to think that the midtroposphere patterns we have found to be linked to large area burnt give some hints on large-scale atmospheric patterns prone to lightning activity over the fire regions.

[43] Our results reveal a strong association at interdecadal timescales (low frequency) between PDO and active fire weather in the fire regions of Canada and Alaska during 1959–1999 (auxiliary material Figures S4b and S4c and Table 2). The dynamics of large fires in fire regions from each side of the Canadian Rocky Mountains were mostly in antiphase with each other, as warm (cool) PDO regime enhances (inhibits) fire weather east of the Canadian Rockies, through an increase in temperatures with its maximum in central Canada [*Minobe*, 1997; *Mantua and Hare*, 2002] and the formation of frequent blocking highs over western North America [*Zhang et al.*, 1997]. The mountain ranges in western Canada play a major role in the large-scale patterns of large fire occurrence through retention of PDO-related Pacific Ocean moisture.

[44] AO and ENSO modulate such long-term trends of large fire activity at interannual timescales (high frequency; Figures 6 and 7 and auxiliary material S4a and S4d). Positive AO enhances fire weather in the midlatitude Fire regions through the presence of midlatitude blocking highs typical of positive AO situations and negative AO enhances fire weather in the northernmost fire regions (Alaska and Northwest Territories) through a southward expansion of the Arctic blocking high. The coincidence of interannual wavelet power in the analysis of fire climate indices and PDO and ENSO indices suggests that both teleconnections do not affect area burnt independently. Interannual ENSO events interact with the interdecadal effects of PDO during El Niño and La Niña events [*Gershunov and Barnett*, 1998; *Brown and Comrie*, 2004]. We refer to PDO (ENSO) when discussing the interdecadal (interannual) variability effects of PDO/ENSO.

[45] PDO regime changed in 1976–1977 from a cool to a warm phase (Figure 5b) [*Trenberth*, 1990; *Trenberth and Hurrell*, 1994], which persisted at least until 1997 [*MacDonald and Case*, 2005]. Such regime shift also occurred in ENSO [*Quinn and Neal*, 1984, 1985; *Nitta and Yamada*, 1989]. Dramatic ecological shifts over North America have been reported to be associated with this regime shift [*Venrick et al.*, 1987; *Roemmich and McGowan*, 1995; *Hare et al.*, 1999]. Yearly area burnt totals differ strongly prior to and after 1976 in all fire regions except for Alaska (Figure 3): large fire events frequency increased due to the warm PDO phase and persistent positive AO in all fire regions east of the Canadian Rocky Mountains. On the other hand, area burnt decreased in British Columbia due to the PDO regime shift; no large fires associated with cool PDO occurred there after 1976. Three isolated large fire events occurred in British Columbia under warm PDO situations and were responsible for large fires in the Canadian Rockies (1985) or in the Yukon boundary area (1969). Total area burned in Alaska did not show trends because ~40% of its total area burnt burned associated with negative AO events, which

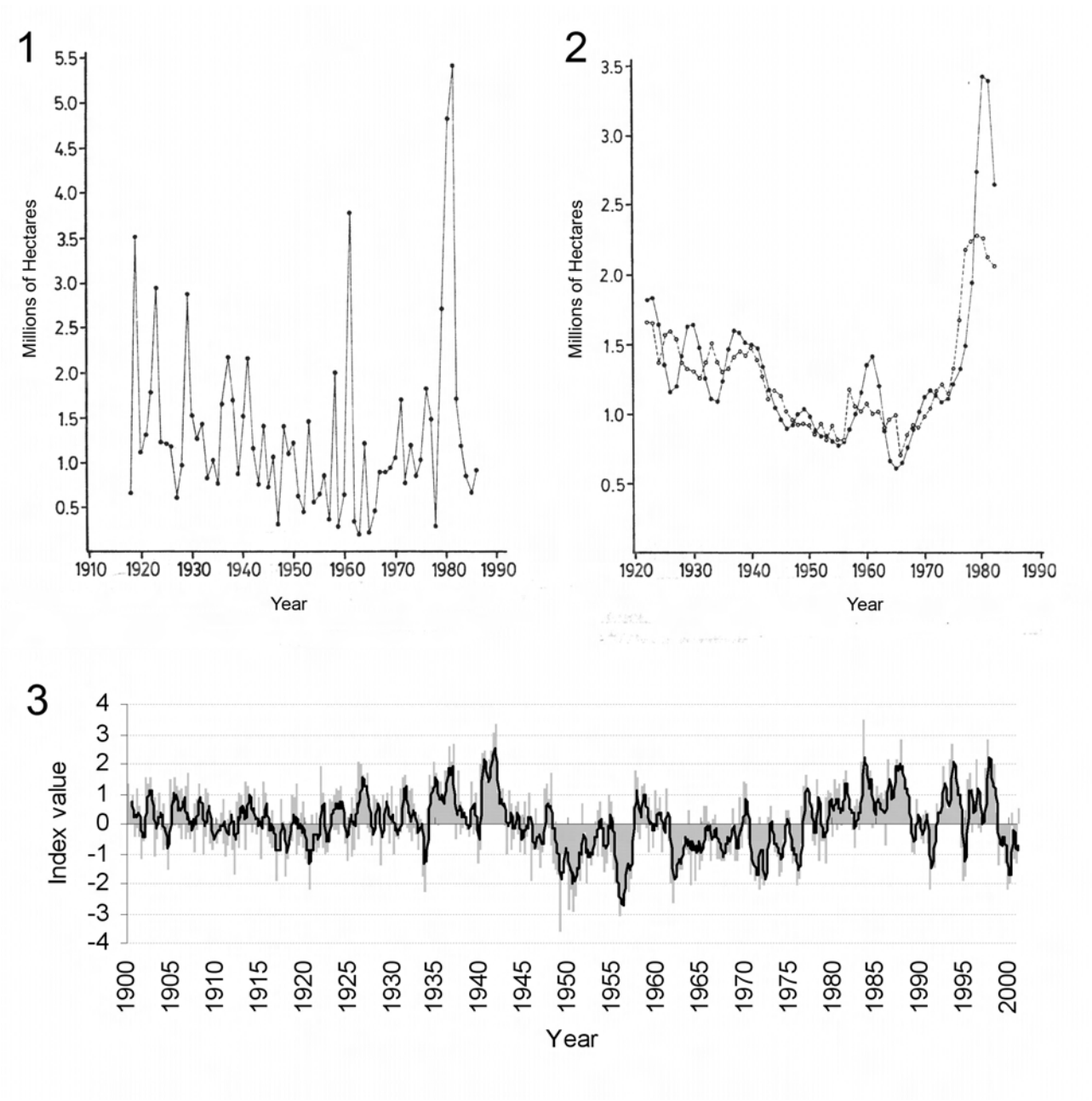

Figure 8. Comparison of the 20th century PDO versus area burnt in Canada. (a) Annual area burned in Canada from 1918–1986 (Figure 1 of *Van Wagner* [1988]). (b) Simple 10-year running mean (dotted line) and exponential mean with a weight of 0.1 in the current year (solid line), both plotted over current year for annual area burned in Canada for the years 1918–1986 (Figure 2 of *Van Wagner* [1988]). (c) Monthly Pacific Decadal Oscillation Index for the period 1900–2000. Thick line corresponds to a 6-month running mean.

were common during the early period of the record, and ~35% of it burned associated with the warm PDO regime after 1976. Previous studies attributed an influence of ENSO, Pacific/North America (PNA) and PDO on large fire activity in interior Alaska [*Hess et al.*, 2001; *Duffy et al.*, 2005]. Our results largely agree with the findings of *Hess et al.* [2001] and show in addition the even stronger influence of AO on large fire occurrence in the region.

[46] Moreover, positive AO-related large fire events occurred only after the PDO regime shift in 1976 (Table 1). Thus, interdecadal PDO variability interacts with interannual AO variability, enhancing large fire occurrence east of the Canadian Rocky Mountains. Large fires associated with AO-induced high-pressure anomalies in midlatitudes tend to occur more frequently under warm PDO regimes as positive air temperature anomalies occur over northern North America during warm PDO events [*Zhang et al.*, 1997; *Minobe*, 1997]. *Bonsal et al.* [2001] suggested that positive PDO/ENSO events during winter would inhibit the flow of cold Arctic air over most of Canada by displacing the polar jet

stream northward through an eastward displacement of the western Canadian Ridge produced by a deeper than normal Aleutian low.

[47] That the phase angles between teleconnection indices and fire climate indices are constant across all time and frequency scales (Table 3) argues for a constant time lag due to the physical mechanism of signal propagation from teleconnections to fire climate indices.

6. Conclusion and Significance

[48] The PDO/ENSO regime shift in 1976 triggered an increase in area burned east of the Canadian Rocky Mountains and, as a result, in the total area burned for the whole study area. Indeed, the correlation between the low-pass-filtered total area burned in Canada and PDO spring-summer time series is 0.7 for the study period. Thus the overall increase in area burned observed in the North American boreal forest (Figure 3) [*Stocks et al.*, 2002; *Gillett et al.*, 2004; *Flannigan et al.*, 2005] resulted mainly from the onset of a warm PDO regime and persistent positive AO situations. Despite increased precipitation in eastern Canada [*Bergeron and Archambault*, 1993; *Tardif and Bergeron*, 1997; *Girardin et al.*, 2004], area burned there also increased after 1976 and during the positive AO events in the late 1980s and 1990s (Figures 3 and 5b). Our results suggest a greater influence of PDO at interdecadal timescales over large fire occurrence in eastern Canada than those of *Girardin et al.* [2004]: 45% of the area burned by large fire events in fire region East was directly associated with PDO-related midtropospheric patterns and the remaining 55%, AO-related, occurred only after the onset of a warm PDO regime in 1976.

[49] PDO regime shifts have occurred previously in the late 19th and the 20th century [*Minobe*, 1997; *Mantua and Hare*, 2002] resulting in warm PDO phases during 1870–1889, 1925–1946 and 1976 to at least 1997 [*Minobe*, 2000; *MacDonald and Case*, 2005], and cool PDO phases during 1890–1924 and 1947–1976. According to our results, overall low (high) large fire activity should have occurred during cool (warm) PDO regimes, with high frequency modulation of large fire occurrence by AO and ENSO events. Studies using Canadian data for a longer period (1918–1990s) confirm our findings (Figure 8) [*Van Wagner*, 1988, Figure 1; *Van Wagner*, 1991] and show extensive area burned from 1927 to 1946, followed by a steady decline from 1946–1947 and a sudden rise from 1976 onward. Long fire records for Canada, such as that of Van Wagner, have been considered deficient in the early years due to underestimation of total area burned in northern Canada [*Stocks et al.*, 2002]; however, they illustrate general trends in total annual area burnt and are the only source of such data. PDO index and these historical area burnt series are strikingly similar, and they even share a short 2–3 year positive peak around 1960 (Figure 8); correlation between the 10-year smoothed annual PDO and Van Wagner's fire totals (as taken from Figure 1 of *Van Wagner* [1988]) is 0.67, whereas the correlation between both annual series is 0.46.

[50] The fire regions formed through the interaction of PDO/ENSO and AO at different timescales. Changes in the dynamics of such teleconnection patterns, especially the PDO, are likely to change the large-scale spatiotemporal patterns of large fire occurrence described in this study. Thus it is important to know whether the PDO has been a consistently robust feature in North Pacific climate, and whether its dominant periodicities have persisted during the last centuries. Reconstructions of the PDO based on tree rings and coral [*Minobe*, 1997; *Biondi et al.*, 2001; *D'Arrigo et al.*, 2001; *Gedalof and Smith*, 2001; *Gedalof et al.*, 2002; *Moore et al.*, 2002; *MacDonald and Case*, 2005] show, despite some contradictions and with the caution needed when interpreting decadal variability taken from such proxy data, that the PDO regime seems to have fluctuated in importance, with notable intervals of weak or even no activity (i.e., 19th century [*Biondi et al.*, 2001; *Gedalof and Smith*, 2001; *Gedalof et al.*, 2002]) and other periods where it was locked into a cool phase for about four centuries (10th to 14th century), causing severe drought all over western North America. These past situations involved a different mean state of the ocean-atmosphere system than that typical today [*MacDonald and Case*, 2005]. Nonlinear dynamics in the ocean-atmosphere system are likely to be the cause of such intermittences at different low-frequency scales [*Overland et al.*, 2000].

[51] This suggests that the spatial and temporal patterns in the occurrence of large fires might have been very different during the past centuries over Canada and Alaska than those observed for 1959–1999, probably causing changes in fire frequency. Indeed, major shifts in fire frequency have been detected during the last centuries [*Reed et al.*, 1998; *Reed*, 2001; *Bergeron et al.*, 2001; *Lesieur et al.*, 2002], which might be related to strong-weak PDO transitions. Evidence of a distinct fire cycle in western Canada during most of the 19th century [*Reed*, 2001] is probably linked to a weak PDO period. The onset of a more energetic interdecadal PDO regime in the late 19th to early 20th centuries [*MacDonald and Case*, 2005; *Gedalof and Smith*, 2001] might be related to changes in fire frequency at the end of the 19th century and the first decades of the 20th century [*Reed*, 2001; *Bergeron et al.*, 2001].

[52] The possibility of a PDO regime reversal between 1997 and 1999 has been reported [*Minobe*, 2000; *MacDonald and Case*, 2005]. To verify that such a regime shift occurred and to determine the nature of the shift requires a careful future examination of additional data in the coming years [*Minobe*, 2000]. Such regime shift would have major implications in total area burned in the area: A negative PDO situation would imply an overall reduction in total area burnt relative to 1977–1997, with the exception of British Columbia, where area burnt would increase. On the other hand, a more variable PDO regime would imply changes in the spatiotemporal patterns of large lightning fires. Thus caution should be exercised when using the multidecadal behavior of the PDO observed in the 20th century instrumental records as a basis for anticipating long-term variability [*MacDonald and Case*, 2005] in the occurrence of large fires beyond the immediate future.

[53] Another global change scenario [e.g., *Gillett et al.*, 2004] predicts higher temperatures and increased of evapotranspiration over North America. This could result not so much in changes in the position of the midtropospheric ridges but in changes in the duration needed to effectively dry fuel.

[54] **Acknowledgments.** This study was supported by a grant for graduate studies in Canada given by "La Caixa" and the International Council of Canadian Studies to Marc Macias Fauria, a NSERC Discovery grant and the G8 Legacy Chair in Ecology given to E. A. Johnson.

[55] We thank very much John Moore and Aslak Grinsted at the University of Lapland (Finland) for comments and assistance. On the Catalan side, we thank Pere Roca-Cusachs for his feedback.

References

Bergeron, Y., and S. Archambault (1993), Decrease of forest fires in Quebec's southern boreal zone and its relation to global warming since the Little Ice Age, *Holocene*, *3*, 255–259.

Bergeron, Y., S. Gauthier, V. Kafka, P. Lefort, and D. Lesieur (2001), Natural fire frequency for the eastern Canadian boreal forest: Consequences for sustainable forestry, *Can. J. For. Res.*, *31*, 384–391.

Biondi, F., A. Gershunov, and D. R. Cayan (2001), North Pacific decadal climate variability since 1661, *J. Clim.*, *14*, 5–10.

Bonsal, B. R., and R. G. Lawford (1999), Teleconnections between El Niño and La Niña events and summer extended dry spells on the Canadian prairies, *Int. J. Climatol.*, *19*, 1445–1458.

Bonsal, B. R., A. Shabbar, and K. Higuchi (2001), Impacts of low frequency variability modes on Canadian winter temperature, *Int. J. Climatol.*, *21*, 95–108.

Brown, D. P., and A. C. Comrie (2004), A winter precipitation 'dipole' in the western United States associated with multidecadal ENSO variability, *Geophys. Res. Lett.*, *31*, L09203, doi:10.1029/2003GL018726.

Carcaillet, C., Y. Bergeron, P. J. H. Richard, B. Fréchette, S. Gauthier, and Y. T. Prairie (2001), Change of fire frequency in the eastern Canadian boreal forests during the Holocene: Does vegetation composition of climate trigger the fire regime?, *J. Ecol.*, *89*, 930–946.

Coulibaly, P., and D. H. Burn (2005), Spatial and temporal variability of Canadian seasonal stream flows, *J. Clim.*, *18*, 191–210.

D'Arrigo, R., R. Villalba, and G. Wiles (2001), Tree-ring estimates of Pacific decadal climate variability, *Clim. Dyn.*, *18*, 219–224.

Díaz, H. F. (1981), Eigenvector analysis of seasonal temperature, precipitation and synoptic-scale system frequency over the contiguous United States: Part II. Spring, summer, fall and annual, *Mon. Weather Rev.*, *109*, 1285–1304.

Duffy, P. A., J. E. Walsh, J. M. Graham, D. H. Mann, and T. S. Rupp (2005), Impacts of large-scale atmospheric-ocean variability on Alaskan fire season severity, *Ecol. Appl.*, *15*, 1317–1330.

Enfield, D. B., A. M. Mestas-Nuñez, and P.-J. Trimble (2001), The Atlantic multidecadal oscillation and its relation to rainfall and river flows in the continental U.S., *Geophys. Res. Lett.*, *28*(10), 2077–2080.

Evans, M. N., A. Kaplan, and M. A. Cane (2000), Intercomparison of coral oxygen isotope data and historical sea surface temperature (SST): Potential for coral-based SST field reconstructions, *Paleoceanography*, *15*(5), 551–563.

Evans, M. N., M. A. Cane, D. P. Schrag, A. Kaplan, B. K. Linsley, R. Villalba, and G. M. Wellington (2001), Support for tropically-driven Pacific decadal variability based on paleoproxy evidence, *Geophys. Res. Lett.*, *28*(19), 3689–3692.

Finklin, A. I. (1973), Meteorological factors in the Sundance fire run, USDA For. Serv. *Gen. Tech. Rep. INT-6*, U.S.D.A. For. Serv., Corvallis, Oreg.

Flannigan, M. D., and J. B. Harrington (1986), Synoptic weather conditions during the Porter Lake experimental fire project, *Climatol. Bull.*, *20*, 19–40.

Flannigan, M. D., K. A. Logan, B. D. Amiro, W. R. Skinner, and B. J. Stocks (2005), Future area burned in Canada, *Clim. Change*, *72*, 1–16.

Gedalof, Z., and D. J. Smith (2001), Interdecadal climate variability and regime-scale shifts in Pacific North America, *Geophys. Res. Lett.*, *28*(8), 1515–1518.

Gedalof, Z., N. J. Mantua, and D. L. Peterson (2002), A multi-century perspective of variability in the Pacific Decadal Oscillation: New insights from tree rings and coral, *Geophys. Res. Lett.*, *29*(24), 2204, doi:10.1029/2002GL015824.

Gershunov, A., and T. P. Barnett (1998), Interdecadal modulation of ENSO teleconnections, *Bull. Am. Meteorol. Soc.*, *79*, 2715–2726.

Gillett, N. P., A. J. Weaver, F. W. Zwiers, and M. D. Flannigan (2004), Detecting the effect of climate change on Canadian forest fires, *Geophys. Res. Lett.*, *31*, L18211, doi:10.1029/2004GL020876.

Girardin, M.-P., J. Tardif, M. D. Flannigan, and Y. Bergeron (2004), Multicentury reconstruction of the Canadian Drought Code from eastern Canada and its relationship with paleoclimatic indices of atmospheric circulation, *Clim. Dyn.*, *23*, 99–115.

Grinsted, A., J. C. Moore, and S. Jevrejeva (2004), Application of the cross wavelet transform and wavelet coherence to geophysical time series, *Nonlinear Proc. Geophys.*, *11*, 561–566, SRef 1607–7946/npg/2004–11–561.

Grumm, R. H., and R. Hart (2001), Standardized anomalies applied to significant cold season weather events: Preliminary findings, *Weather Forecast*, *16*, 736–754.

Hare, S.R. (1996), Low frequency climate variability and salmon production, Ph.D. dissertation, 306 pp., Univ. of Wash., Seattle.

Hare, S. R., N. J. Mantua, and R. C. Francis (1999), Inverse production regimes: Alaskan and West Coast salmon, *Fisheries*, *24*, 6–14.

Hess, J. C., C. A. Scott, G. L. Hufford, and M. D. Fleming (2001), El Nino and its impact on fire weather conditions in Alaska, *Int. J. Wildland Fire*, *10*, 1–13.

Hoerling, M., and A. Kumar (2003), The perfect ocean for drought, *Science*, *299*, 691–694, doi:10.1126/science.1079053.

Janz, B., and N. Nimchuk (1985), The 500mb chart—A useful fire management tool, paper presented at 8th Conference on Fire and Forest Meteorology, Soc. of Am. For., Washington, D. C.

Jevrejeva, S., J. C. Moore, and A. Grinsted (2003), Influence of the Arctic Oscillation and El Niño–Southern Oscillation (ENSO) on ice conditions in the Baltic Sea: The wavelet approach, *J. Geophys. Res.*, *108*(D21), 4677, doi:10.1029/2003JD003417.

Johnson, E. A. (1992), *Fire and Vegetation Dynamics: Studies from the North-American Boreal Forest*, Cambridge Univ. Press, New York.

Johnson, E. A., and C. P. S. Larsen (1991), Climatically induced change in fire frequency in the southern Canadian Rockies, *Ecology*, *72*, 194–201.

Johnson, E. A., and D. R. Wowchuck (1993), Wildfires in the southern Canadian Rocky Mountains and their relationship to mid-tropospheric anomalies, *Can. J. For. Res.*, *23*, 1213–1222.

Kaiser, H. F. (1958), The VARIMAX criterion for analytical rotation in factor analysis, *Psychometrika*, *23*, 187–201.

Kalnay, E., et al. (1996), The NCEP/NCAR 40–year reanalysis project, *Bull. Am. Meteorol. Soc.*, *77*, 437–471.

Kiladis, G. N., and H. F. Diaz (1989), Global climatic anomalies associated with extremes in the Southern Oscillation, *J. Clim.*, *2*, 1069–1090.

Knox, J. L., and R. G. Lawford (1990), The relationship between Canadian prairie dry and wet months and circulation anomalies in the mid-troposphere, *Atmos. Ocean*, *28*, 189–215.

Larsen, C. P. S. (1997), Spatial and temporal variations in boreal forest fire frequency, *J. Biogeogr.*, *24*, 663–673.

Lesieur, D., S. Gauthier, and Y. Bergeron (2002), Fire frequency and vegetation dynamics for the south-central boreal forest of Quebec, Canada, *Can. J. For. Res.*, *32*, 1996–2009.

Levine, J. S. (Ed.) (1996), *Global Biomass Burning: Atmospheric, Climatic, and Biospheric Implications*, MIT Press, Cambridge, Mass.

Linsley, B. K., G. M. Wellington, and D. P. Schrag (2000), Decadal sea surface temperature variability in the subtropical South Pacific from 1726 to 1997 A.D., *Science*, *290*, 1145–1148.

MacDonald, G. M., and R. A. Case (2005), Variations in the Pacific Decadal Oscillation over the past millennium, *Geophys. Res. Lett.*, *32*, L08703, doi:10.1029/2005GL022478.

Mantua, N. J., and S. R. Hare (2002), The Pacific Decadal Oscillation, *J. Oceanogr.*, *58*, 35–44.

Mantua, N. J., S. R. Hare, Y. Zhang, J. M. Wallace, and R. C. Francis (1997), A Pacific interdecadal climate oscillation with impacts on salmon production, *Bull. Am. Meteorol. Soc.*, *78*, 1069–1079.

Masters, A. M. (1990), Changes in forest fire frequency in Kootenay National Park, Canadian Rockies, *Can. J. Bot.*, *68*, 1763–1767.

Minobe, S. (1997), A 50–70 year climatic oscillation over the North Pacific and North America, *Geophys. Res. Lett.*, *24*(6), 683–686.

Minobe, S. (2000), Spatio-temporal structure of the pentadecadal variability over the North Pacific, *Prog. Oceanogr.*, *47*, 381–408.

Moore, G. W. K., G. Holdsworth, and K. Alverson (2002), Climate change in the North Pacific region over the past three centuries, *Nature*, *240*, 401–403.

Nash, C. H., and E. A. Johnson (1996), Synoptic climatology of lightning-caused forest fires in the subalpine and boreal forests, *Can. J. For. Res.*, *26*, 1859–1874.

Nitta, T., and S. Yamada (1989), Recent warming of tropical sea surface temperature and its relationship to the Northern Hemisphere circulation, *J. Meteorol. Soc. Jpn.*, *67*, 187–193.

Overland, J. E., J. M. Adams, and H. O. Mofjeld (2000), Chaos in the North Pacific: Spatial modes and temporal irregularity, *Prog. Oceanogr.*, *47*, 337–354.

Quinn, W. H., and V. T. Neal (1984), Recent climate change and the 1982–83 El Niño, paper presented at Eighth Annual Climate Diagnostic Workshop, Natl. Oceanic and Atmos. Admin., Downsville, Ont., Canada.

Quinn, W. H., and V. T. Neal (1985), Recent long-term climate change over the eastern tropical and sub-tropical Pacific and its ramifications, paper presented at Ninth Annual Climate Diagnostic Workshop, Natl. Oceanic and Atmos. Admin., Corvallis, Oreg.

Rajagopalan, B., E. Cook, U. Lall, and B. K. Ray (2000), Spatiotemporal variability of ENSO and SST teleconnections to summer drought

over the United States during the twentieth century, *J. Clim.*, *13*, 4244–4255.
Reed, W. J. (2001), Statistical inference for historical fire frequency using the spatial mosaic, in *Forest Fires: Behaviour and Ecological Effects*, edited by E. A. Johnson and K. Miyanishi, pp. 419–436, Elsevier, New York.
Reed, W. J., C. P. S. Larsen, E. A. Johnson, and G. M. MacDonald (1998), Estimation of temporal variations in historical fire frequency from time-since-fire map data, *For. Sci.*, *44*(3), 465–475.
Richman, M. B., and P. J. Lamb (1985), Climatic pattern analysis of three- and seven-day summer rainfall in the central United States: Some methodological considerations and a regionalization, *J. Clim. Appl. Meteorol.*, *24*, 1325–1343.
Richman, M. B., and P. J. Lamb (1987), Pattern analysis of growing season precipitation in southern Canada, *Atmos. Ocean*, *25*, 137–158.
Roemmich, D., and J. McGowan (1995), Climatic warming and the decline of zooplancton in the California current, *Science*, *267*, 1324–1326.
Ropelewski, C. F., and M. S. Halpert (1986), North American precipitation and temperature patterns associated with El Niño/Southern Oscillation (ENSO), *Mon. Weather Rev.*, *114*, 2352–2362.
Ropelewski, C. F., and M. S. Halpert (1987), Global and regional scale precipitation patterns associated with the El Niño/Southern Oscillation, *Mon. Weather Rev.*, *115*, 1606–1626.
Rummel, R. J. (1970), *Applied Factor Analysis*, pp 349–367, Northwestern Univ. Press, Evanston, Ill.
Schroeder, M. J., et al. (1964), Synoptic weather types associated with critical fire weather, report, Pac. Southwest For. and Range Exper. Stn., USDA For. Serv., Berkeley, Calif.
Serreze, M. C., M. P. Clark, and D. L. McGinnis (1998), Characteristics of snowfall over the eastern half of the United States and relationships with principal modes of low-frequency atmospheric variability, *J. Clim.*, *11*, 234–250.
Shabbar, A., and W. Skinner (2004), Summer drought patterns in Canada and the relationship to global sea surface temperatures, *J. Clim.*, *17*, 2866–2880.
Shabbar, A., B. Bonsal, and M. Khandekar (1997), Canadian precipitation patterns associated with the Southern Oscillation, *J. Clim.*, *10*, 3016–3027.
Skinner, W. R., B. J. Stocks, D. L. Martell, B. Bonsal, and A. Shabbar (1999), The association between circulation anomalies in the mid-troposphere and area burned by wildland fire in Canada, *Theor. Appl. Climatol.*, *63*, 89–105.
Skinner, W. R., M. D. Flannigan, B. J. Stocks, D. L. Martell, B. M. Wotton, J. B. Todd, J. A. Mason, K. A. Logan, and E. M. Bosch (2002), A 500hPa synoptic wildland climatology for large Canadian Forest Fires, 1959–1996, *Theor. Appl. Climatol.*, *71*, 157–169.
Sneath, P. H., and R. R. Snokal (1973), *Numerical Taxonomy*, pp. 230–234. W. H. Freeman, New York.
Stocks, B. J., et al. (1998), Climate change and forest fire potential in Russian and Canadian boreal forests, *Clim. Change*, *38*, 1–13.
Stocks, B. J., et al. (2002), Large forest fires in Canada, 1959–1997, *J. Geophys. Res.*, *107*, 8149, doi:10.1029/2001JD000484. [printed 108(D1), 2003].
Street, R. B. (1985), Drought and synoptic fire climatology of the boreal forest region of the Canadian Prairie Provinces, paper presented at 8th Conference on Fire and Forest Meteorology, Soc. of Am. For., Washington, D. C.
Tardif, J., and Y. Bergeron (1997), Ice-flood history reconstructed with tree-rings from the southern boreal forest limit, western Québec, *Holocene*, *7*, 291–300.
Thompson, D. W. J., and J. M. Wallace (2001), Regional climate impacts of the Northern Hemisphere annular mode, *Science*, *293*, 85–89.
Torrence, C., and G. P. Compo (1998), A practical guide to wavelet analysis, *Bull. Am. Meteorol. Soc.*, *79*, 61–78.
Trenberth, K. E. (1990), Recent observed interdecadal climate changes in the Northern Hemisphere, *Bull. Am. Meteorol. Soc,.*, *71*, 988–993.
Trenberth, K. E., and G. W. Branstator (1992), Issues in establishing causes of the 1988 drought over North America, *J. Clim.*, *5*, 303–309.
Trenberth, K. E., and W. Hurrell (1994), Decadal atmospheric-ocean variations in the Pacific, *Clim. Dyn.*, *9*, 303–309.
Trenberth, K. E., and D. A. Paolino (1981), Characteristic patterns of variability of sea-level pressure in the Northern Hemisphere, *Mon. Weather Rev.*, *109*, 1169–1189.
Van Wagner, C. E. (1987), The development and structure of the Canadian Forest Fire Weather Index System, *For. Tech. Rep. 35*, Can. For. Serv., Ottawa, Ont., Canada.
Van Wagner, C. E. (1988), The historical pattern of annual burned area in Canada, *For. Chron.*, *64*, 182–185.
Van Wagner, C. E. (1991), Forest fire statistics and the timber supply, in *Canada's Timber Resources*, edited by D. G. Brand, *Rep. PI-X-101*, pp. 111–118, For. Can. Inf., Chalk River, Ont., Canada.
Venrick, E. L., J. A. McGowan, D. R. Cayan, and T. L. Hayward (1987), Climate and chlorophyll *a*: Long-term trends in the central north Pacific Ocean, *Science*, *238*, 70–72.
Wallace, J. M., and D. S. Gutzler (1981), Teleconnections in the geopotential height field during the Northern Hemisphere winter, *Mon. Weather Rev.*, *109*, 784–812.
Walsh, J. E., and A. Mostek (1980), A quantitative analysis of meteorological anomaly patterns over the United States, 1900–1977, *Mon. Weather Rev.*, *108*, 615–630.
Weir, J. M. H., E. A. Johnson, and K. Miyanishi (2000), Fire frequency and the spatial age mosaic of the mixed-wood boreal forest in western Canada, *Ecol. Appl.*, *10*, 1162–1177.
Xue, X., T. M. Smith, and R. W. Reynolds (2003), Interdecadal changes of 30–yr SST normals during 1871–2000, *J. Clim.*, *16*, 1601–1612.
Yarnal, B. (1984), Relationships between synoptic-scale atmospheric circulation and glacier mass balance in south-western Canada during the International Hydrological Decade, 1965–74, *J. Glaciol.*, *30*(105), 188–198.
Zhang, X., L. A. Vincent, W. D. Hogg, and A. Niitsoo (2000), Temperature and precipitation trends in Canada during the 20th century, *Atmos. Ocean*, *38*, 395–429.
Zhang, Y., J. M. Wallace, and D. S. Battisti (1997), ENSO-like interdecadal variability: 1900–93, *J. Clim.*, *10*, 1004–1020.

M. Macias Fauria, Department of Ecology, Faculty of Biology, University of Barcelona, Av. Diagonal 645, E-08028 Barcelona, Spain. (marc.macias@helsinki.fi)

E. A. Johnson, Department of Biological Sciences, University of Calgary, 2500 University Drive N.W., Calgary, Alberta, Canada T2N 1N4. (johnsone@ucalgary.ca)